Journal of Energy Storage 87 (2024) 111267

Contents lists available at ScienceDirect

Journal of Energy Storage

journal homepage: www.elsevier.com/locate/est

Research Papers

Mathematical expressions for simulation of supercapacitor voltammetry curves and capacitance dependence on scan rate

Fernando Gabriel, Jara Benitez [a,b,*], Alejandro Jorge, Bardella Peruzzi [b], Rubens Nunes Faria Jr [a]

[a] Nuclear and Energy Research Institute - São Paulo (IPEN-SP), Brazil
[b] Facultad Politécnica - Universidad Nacional del Este – FPUNE, Ciudad del Este, Alto Paraná, Brazil

ARTICLE INFO

Keywords:
Supercapacitors
Voltammetry curves
Capacitance dependence on scan rates
Simulation

ABSTRACT

A straightforward RC series circuit model was proposed to fit the cyclic voltammetry experimental data of various symmetrical electrochemical supercapacitors. The model simulated the experimental behavior for exponential dependence of capacitance on the scan rate. In this model, the zero-scan rate capacitance was considered as a constant, and the equivalent serial resistance depended on the scan rate. Neither the equivalent parallel resistance nor a possible intrinsic dependence of capacitance on applied voltage was considered in the modelling.

1. Introduction

Among the different energy storage and conversion technologies, electrochemical systems, such as batteries, fuel cells, and electrochemical capacitors (EC) have received considerable attention in recent years owing to the growth in global energy demand. In particular, ECs, also known as electrochemical double-layer capacitors (EDLCs), can store energy at a relatively higher energy density than conventional capacitors. EDLCs have been used in a wide range of applications in electric and hybrid vehicles, electronic communication devices, aircrafts, and smart grids. Several advantages attributed to the application of EDLCs include fast charging, long charge-discharge cycles, and a wide operating temperature range [1]. Supercapacitors store charges at the porous surface interface between two electrodes immersed in an electrolyte solution. Each electrode-electrolyte interface can be represented by a capacitor such that the whole cell can be considered as two connected series capacitors, C_1 and C_2 [2,3]. For a symmetrical capacitor (electrodes of the same material), the total cell capacitance (C_{Cell}) can be calculated as

$$\frac{1}{C_{Cell}} = \frac{1}{C_1} + \frac{1}{C_2} = \frac{2}{C_T} \tag{1}$$

Capacitance is an important parameter defining EC performance, along with the equivalent series resistance (ESR), energy density, power density, time, and operating voltage. In general, three techniques are used to evaluate EC performance, which aim to assess the electrochemical characteristics of the EC from different points of view, including capacitance. CV is a technique in which the current response is measured at a fixed voltage scan rate. Second, galvanostatic charge/discharge (CG) uses a fixed current density to obtain a voltage variation as a response, and electrochemical impedance spectroscopy (EIS) measures the impedance of a cell as a function of frequency by applying a low-amplitude alternating voltage superimposed on a steady-state potential [4,5].

Abbreviations: C_{eff}, Effective capacitance resulting from the proposed model; C_o, Characteristic capacitance, a parameter obtained with the model; $I_{\#}$, Intensity of the time-dependent electric current supplied by the direct current source I (in this case, the voltammogram source), unit: ampere (A), $\# = 0,1,2,3\ldots$; $Q_{\#}$, Electric charge values, # = I, II, III, IV, V, ….; R_s, Serial resistance; V_m, Maximum potential reached in a voltammetric measurement; ν_o, Scan rate characteristic of each capacitor; $\lambda^{\#} = e^{-\frac{T}{\tau}}$, # = 0,1,2,3…; C, Fixed capacitance; farad (F), Capacitance obtained from the area of the voltammogram; I, Intensity of the electric current supplied by the direct current source I (in this case, the voltammogram source) (A); R (ESR), Represents the equivalent series resistance; ohm (Ω), The series resistance obtained through the technique of abrupt variation of the electric potential; t, Elapsed time of the charging and discharging processes of a supercapacitor (s); V(t), Electric potential between the terminals of an electrochemical supercapacitor evaluated using the cyclic voltammetry technique at each moment of its charging or discharging process, in units: volt (V); $I(t)$, Intensity of the time-dependent electric current supplied by the direct current source I (in this case, the voltammogram source) in units: ampere (A); T, Time interval in which the value of the maximum potential V_m is reached or the semi-period of each cycle; ν, Scanning rate used in voltammetry technique; τ, Characteristic time constant defined by the *RC* serial circuit association.

* Corresponding author at: Nuclear and Energy Research Institute - São Paulo (IPEN-SP), Brazil.
E-mail address: fernando.benitez@usp.br (F.G.J. Benitez).

https://doi.org/10.1016/j.est.2024.111267
Received 20 December 2023; Received in revised form 14 February 2024; Accepted 10 March 2024
Available online 27 March 2024

From the CV tests, the capacitance depends on scan rate. However, few studies have focused on analyzing this capacitance behavior. Capacitance decreased exponentially with increasing scan rate. Wehmeyer and Wightman first adopted this approach [6]. They studied the dependence of apparent capacitance on scanning rate in microvoltammetric, disk-shaped electrodes embedded in an infinite insulation plane, sealed with soft glass or epoxy, with the surface exposed by polishing with various types of abrasives. They highlighted that the quality of electrode seal was most noticeable at low frequencies (or scan rates), thus developing a method to improve the quality of voltammetric data on microvoltammetric electrodes when used at low scan rates. Therefore, the dependence of capacitance on scan rate is consistent with the presence of imperfections in the sealing material. This results in an increased voltage drop *iR* which, if sufficiently large, reduces the voltage change in the cracks, thus decreasing the electrode area. Authors considered R_1 as solution resistance, R_2 as leakage resistance, C as electrode capacitance, E as the applied potential, and v the scan rate. To adjust the data obtained, they found an equivalent circuit comprising a resistor in series with a parallel combination of a capacitor and a resistor appropriately modelled to the results, and arrived at an equation that calculates the apparent capacitance by mathematical operations:

$$C_d = \frac{E}{(R_1 + R_{2)}v} + \frac{R_2 C}{(R_1 + R_{2)}} \tag{2}$$

However, Ardizzone et al. [7] verified that the variation in charge q^* with v, the potential sweep rate, proved to be linearizable as a function of $v^{-1/2}$. Thus, it is possible to extrapolate the values of q^* for $v = 0$ and $v = \infty$, respectively. Extrapolation allows an "inner" surface to be considered separately from an "outer" surface in terms of capacitance. The former comprises hard-to-reach regions of proton donor species that assist in surface redox reactions. Assuming that the v-dependence of q^* involves slow access of protons to the "inner" regions of surface, q^* is expected to be a function of the diffusion time. Although this can be strictly defined only in the case of potential-step experiments, the scan rate v can be assumed to be inversely proportional to the diffusion time. This dependence of the numerical values of the interfacial capacitance, in both double-layer and pseudocapacitance, due to surface redox reactions on the charge/discharge current and scan rate, particularly occurs because of the limited diffusion velocity of ions required for charge compensation at the electrochemical interface. In particular, the occupation of electrochemical interface area of the ions within porous structures (internal electrode surface area) decreased with increasing scan rate [8].

Recently, Fernandez et al. [9] showed mathematically that the capacitance of EDCLs depends on the applied potential. They considered a more complete circuit than that proposed in this study, introducing an equivalent parallel resistance (EPR) and capacitor depending on the applied voltage. Although the circuit was more detailed, they did not analyze the possibility of dependence of the capacitance and resistance on scan rate, contrary to this study, in which a constant capacitance and scan-rate-dependent ESR were proposed.

The simplest and most complete model used considers an equivalent circuit comprising a resistor associated in parallel (EPR) with a capacitor, which is associated in series with another resistor (ESR) [10]. The EPR accounts for the self-discharge process that occurs when the capacitor is disconnected from any external circuit, and the ESR accounts for the power loss due to the Joule effect, which is present in any electrical charge diffusion process. In this study, a simple model of the dependence of capacitance on scanning rate from voltammetric data is proposed. Because the behavior of a capacitor in the permanent charge and discharge processes is being studied, the self-discharge process is not considered. This model allows the quantitative analysis of the performance of electrochemical double-layer capacitors, considering the electrode/electrolyte system as a series of RC associations between a resistor and capacitor. Thus, to simplify the analysis, the EPR is considered infinite by this model (usually the EPR values are in the order of 5.10^5 Ω, which yields a discharge Tau of 5.10^5 *s*, while the longest voltammetry period is 1.10^3 s). The ESR, along with the capacitance, defines a time constant, τ. The higher the τ, the lower the charge stored in a given voltammetric period. Therefore, it is important to properly characterize the ESR. Because there are a variety of electrode porosity sizes, a variety of ESR values, and therefore, tau constants, can be expected. Thus, for the present model, we hypothesize that the apparent capacitance is a function of the effective ESR for a given scan rate.

2. Modelling the capacitance dependence on the scan rate

In this study, the electrode-porous/electrolyte system was considered as an ideal series *RC* circuit, in which the relation of the scanning rate v of voltammetry to the time constant $\tau = RC$ determines the current response, and then the charging process. In this context, the equation representing the capacitor charging process can be written as

$$RI + \frac{Q}{C_0} = V(t) = vt \tag{3}$$

where I and Q are the electric charging current and charge of the capacitor at time t, respectively. R is the resistance in series with the ideal capacitance C_0 that represents the maximum occupied area accessible to the ions. In addition, v represents the scan rate of the time-dependent potential $V(t)$, applied to the system during a cyclic voltammetry test. As $I = dQ/dt$, and eq. (3) is derived as

$$\frac{dI}{dt} + \frac{I}{\tau} = \frac{v}{R} \tag{4}$$

whose solution, assuming that the current is initially zero ($I(0) = 0$), is:

$$I(t) = vC_0\left(1 - e^{-\frac{t}{\tau}}\right) \tag{5}$$

By integrating eq. (5) between $t_1 = 0$ and $t_2 = T$, being, T the time interval in which the value of the maximum potential is reached ($V_m = v\,T$), the charge $Q(T)$ corresponding to this potential can be obtained. If the charge $Q(T)$ is divided by V_m, we obtain the effective capacitance C_{eff}:

$$C_{eff} = \frac{Q(\mathrm{T})}{V_m} = C_o\left(1 - \frac{\tau}{T}\left(1 - e^{\frac{-T}{\tau}}\right)\right) \tag{6}$$

Analysis of the first half-cycle charging of a supercapacitor in a voltammetry test

Eqs. (5) and (6) allow the determination of the ideal parameters R and C_o of a capacitor subjected to only the first charging ramp of a supercapacitor subjected to a voltammetry test. By considering $t = T$ in the current eq. (5), the expression for the maximum current of the first cycle is obtained:

$$I_1 = I(T) = vC_0\left(1 - e^{-\frac{T}{\tau}}\right) \tag{7}$$

To express this equation as a function of the scan rate v, we divide the numerator and denominator of τ/T between V_m. Thus, noting that $\frac{T}{V_m} = \frac{1}{v}$, and denoting $\frac{\tau}{V_m} = \frac{1}{v_0}$, eqs. (5) and (6) become

$$I_1 = I(v) = vC_0\left(1 - e^{-v_o/v}\right) \tag{8}$$

$$C_{ef}\,(v) = C_0\left(1 - \frac{v}{v_0}\left(1 - e^{\frac{-v_o}{v}}\right)\right) \tag{9}$$

Eqs. (8) and (9) are schematically presented in Fig. 1: They showed the effects of v_o and ESR on the behavior of I_1 and the capacitance. Increasing *ESR*, or decreasing v_o, increases the value of I_1 and capacitance for a given scan rate, which extends the damping effect of scan rate. Parameter v_0 is the scan rate at which C_{eff} reduces to 37% of C_0, or the time at which current reaches 63 % of the steady-state value, which would arrive under the condition of permanent charging at a linearly

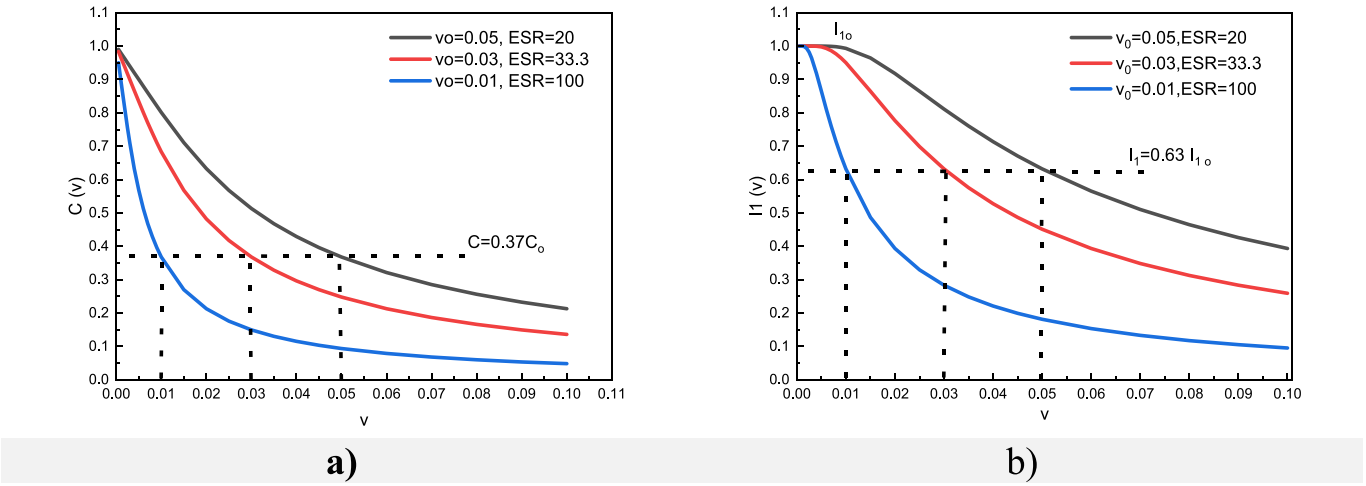

Fig. 1. Schematics representation of eq. 9 (a) and eq. 8 (b).

increasing voltage.

$$v_o = \frac{V_m}{RC_0} = \frac{V_m}{\tau} \tag{10}$$

Eq. 8 is intended to be a simple and effective tool to interpret and analyze the observed dependence of the capacitance (determined in voltammetry) on scanning rate used in the assay, precisely, on that obtained from charging process of the first semi-cycle and assuming an initial current $I(0) = 0$. This model provides parameters that allow to quantitatively compare supercapacitors, and its validity is conditioned to that $EPR/ESR \geq 10000$. In the next subsection, we study the case of complete cycles assuming, for generality, that $I(0)$ is not zero.

Review of subsequent cycles

If we return to eq. (4) with no assumption that I_o is equal to zero and covers a complete cycle, we obtain the following solution:

$$I \pm u = (I_o \pm u)\, e^{-\frac{t-t_o}{\tau}} \tag{11}$$

where $u = \nu C_o$ with ν as the scan rate and $\tau = RC_o$ with C_o as the maximum capacitance of the capacitor with scanning rate tending to zero. I_o is the current from instant t_o, at the beginning of the semicircle. The $(+)$ sign indicates that the potential increases in the 1st half cycle, and the $(-)$ sign indicates that the potential decreases in the 2nd half cycle.

This analysis can be extended to subsequent half-cycles to obtain a general expression for the initial and final currents of the half-cycles. Considering the nth half cycle, the expressions for these currents can be obtained using eq. 12.

$$\begin{aligned} I_{n+1} - u &= (I_n - u)\lambda; \quad n - even \rightarrow n + 1 - odd\ (+v) \\ I_{n+1} + u &= (I_n + u)\lambda; \quad n - odd \rightarrow n + 1 - even\ (-v) \end{aligned} \tag{12}$$

Here, I_n is the starting current of the half-cycle n and I_{n+1} is that of the following half-cycle, T is the time spent in the half-period, and λ is:

$$\lambda = e^{-\frac{T}{\tau}} \tag{13}$$

Eqs. (12) are used to generate the matrix (presented in Table 1) whose elements contain coefficients of the polynomial expressions of the I_n as a function of the parameter λ.

For example, the third row is the expression:

$$\frac{I_2}{u} = -\lambda^0 + 2\lambda^1 - \lambda^2 \tag{14}$$

where I_2 corresponds to the initial current of the third half-cycle, that is, the beginning of the second cycle. Thus, the expressions of the currents as a function of time t, for the first to fourth half cycles are listed in Table 2.

Table 1
Matrix of coefficients of the polynomial expressions of the I_n as a function of λ

	λ^0	λ^1	λ^2	λ^3	λ^4	λ^5	…
$\frac{I_o}{u}$	0	0	0	0	0	0	…
$\frac{I_1}{u}$	1	−1	0	0	0	0	…
$\frac{I_2}{u}$	−1	2	−1	0	0	0	…
$\frac{I_3}{u}$	1	−2	2	−1	0	0	…
$\frac{I_4}{u}$	−1	2	−2	2	−1	0	…
$\frac{I_5}{u}$	1	−2	2	−2	2	−1	…
⋮	⋮	⋮	⋮	⋮	⋮	⋮	⋱

Table 2
Equations used to generate the graph in Fig. 3.

Order of half cycle	Equation	Time interval
1st	$I(t) = (I_0 - u)^* e^{-\frac{t-0}{\tau}} + u$	Para $0T < t < 1T$
2nd	$I(t) = (I_1 + u)^* e^{-\frac{t-T}{\tau}} - u$	Para $1T < t < 2T$
3rd	$I(t) = (I_1 - u)^* e^{-\frac{t-2T}{\tau}} + u$	Para $2T < t < 3T$
4rth	$I(t) = (I_2 + u)^* e^{-\frac{t-3T}{\tau}} - u$	Para $3T < t < 4T$
⋮	⋮	⋮

The current curve I(t) for the second cycle, shown in Fig. 2, was obtained by integrating the equations listed in Table 1. By integrating curve I(t), we obtain the expression for load Q corresponding to the second cycle (refer to eq. 15).

Thus, the charging during the second cycle (eq. 16):

$$Q_{II} = u\left(\tau(1-\lambda)\left(-4+4\lambda-3\lambda^2+\lambda^3\right)+2T\right) \tag{16}$$

with which it was possible to calculate the voltammetric capacitance corresponding to the second cycle (eq. 17).

$$C_{II}(v) = \frac{Q_{II}}{2V_m} = \frac{u}{2V_m}\left(\tau(1-\lambda)\left(-4+4\lambda-3\lambda^2+\lambda^3\right)+2T\right) \tag{17}$$

The integration of current in the time domain is equivalent to that in the potential domain, which is commonly used to calculate the area of voltammogram at which the same capacitance value is reached (eq. 18).

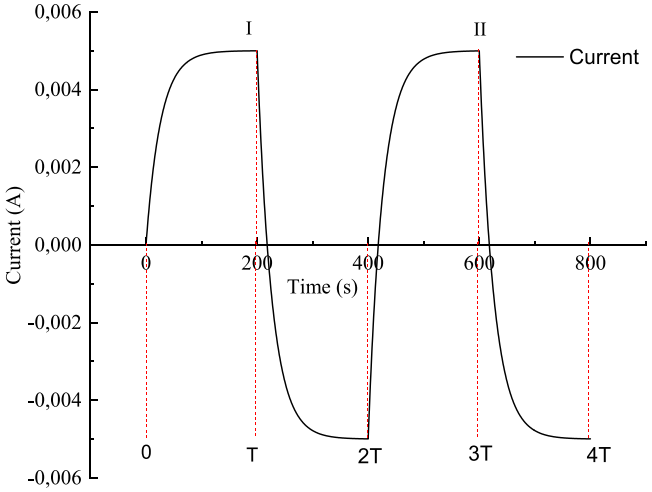

Fig. 2. Current vs. time curve in a cyclic voltammetry process. Two cycles are observed, each consisting of two half cycles.

$$Q_{II} = \int_{2T}^{3T} I(t)dt - \int_{3T}^{4T} I(t)dt \tag{15}$$

$$C = \frac{\int_0^V I(V)dV}{2v\Delta V} \tag{18}$$

where $\Delta V = V_m$.

3. Simulating voltammetry curves with the *RC* model

To simulate a voltammetric charge/discharge process, we can consider a theoretical quasi-ideal SC with $1\,F$ capacitance and three values of *ESR*. For practical purposes, we consider a maximum voltage of $1\,V$. The scan rates selected for the voltammetric simulations were $1, 5, 10, 20, 50$, and $100\,mV/s$. Fig. 3 shows the voltammogram obtained at $v = 1mV/s$.

Procedure to fit the curve C(v) to experimental data.

The rate of charging process is expected to depend on the porosity of electrode. Therefore, for a short $T-$ *time*, the larger pores are preferentially electrically charged. For longer $T-$ *time*, smaller pores are also electrically charged. Therefore, the *ESR*, which depends on the porosity size, has an effective value that depends on T and subsequently on the scan rate v. Consequently, it is not possible to consider the ESR as a constant value; thus, a formula for the variation in ESR with scan rate was obtained. The following formula is used for this purpose:

$$v_0 = v_{01}\left(1 - e^{-\frac{v_{trans}}{v}}\right) + v_{02}\left(e^{-\frac{v_{trans}}{v}}\right) \tag{19}$$

where v_{01} is the value used to fit the lower experimental values of v and v_{02} is the larger value. Exponential factors were used to vary v_o between these extreme values. Parameter v_{trans} is used as the adjustment variable for the fitting processes, which satisfies the condition $v_{01} < v_{trans} < v_{02}$. Fig. 4 shows examples of the use of Eq. 20 to interpolate extreme values of v_o and *ESR*.

$$ESR = \frac{V_m}{C_o v_o} \tag{20}$$

Finally, the expression used to adjust the dependence of the capacitance on the scan rate is

$$C[F] = C_o\left(\left(\frac{v}{v_o}\right)(1-\lambda)\left(-4+4\lambda-3\lambda^2+\lambda^3\right)+2\right) \tag{21}$$

where it becomes $\lambda = e^{-v_o/v}$. To make the fitting of $C(v)$, the capacitance of the second cycle was used to fit C (v).

The fitting parameters used were C_o and v_o (*ESR*). C_o was obtained by extrapolating the experimental curve at a zero scan rate. This can also be performed in subsequent cycles. To use v_o as the adjustment variable, eq. 20 is used to obtain v_{01} and v_{02}, as explained above, with v_{trans} as the final adjustment variable.

Using eq. 21, a simulation that showed the dependence of the capacitance on the scanning rate was performed, as shown in Fig. 5. The same v_o values used for the voltammograms of Fig. 3 were used.

In the same manner, the simulation was performed with the values $v_o = 100, 160, and\ 400$ of Fig. 3, varying the applied potential in the range of $0.5\ V$ to $2.5\ V$. In addition to the dependence of the capacitance on the scanning rate, an increase in the capacitance with applied potential was observed. In contrast to the study by Fernandez et al. (2020) [9], where the capacitance dependence was linear, it was observed that the capacitance did not increase linearly. At higher scanning rates,

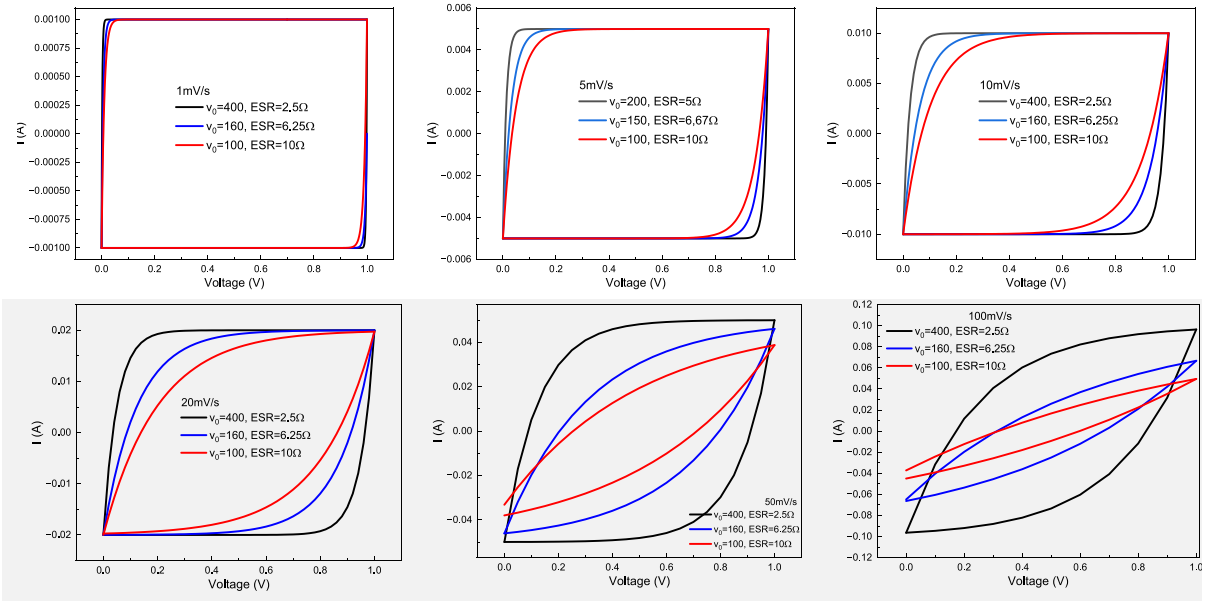

Fig. 3. Example of voltammogram generated with different scan rates and different v_o values.

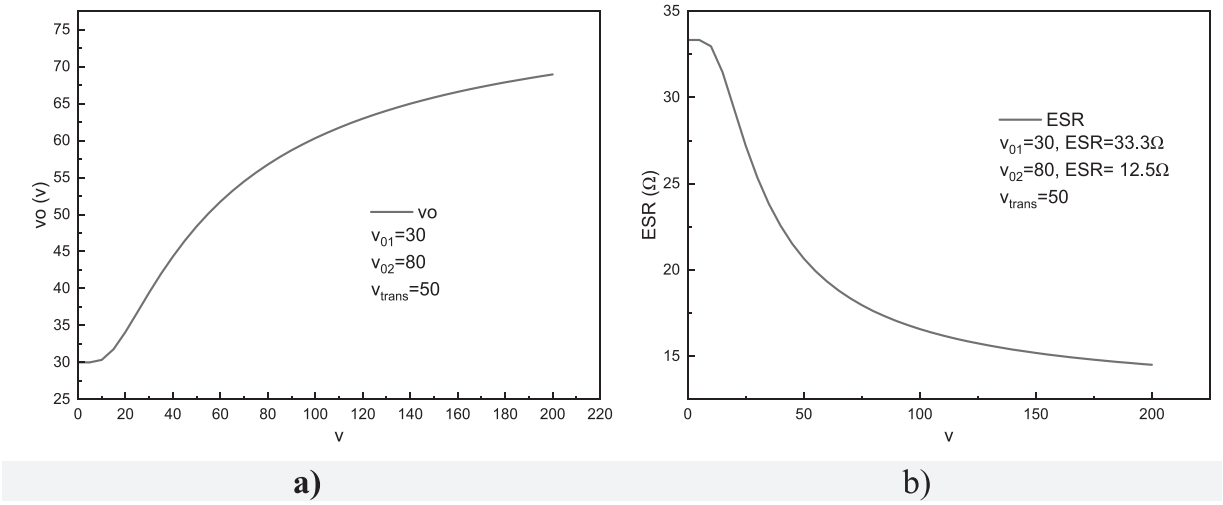

Fig. 4. a) Representation of the interpolation of the extreme values of v_o and b) representation of the interpolation for *ESR*.

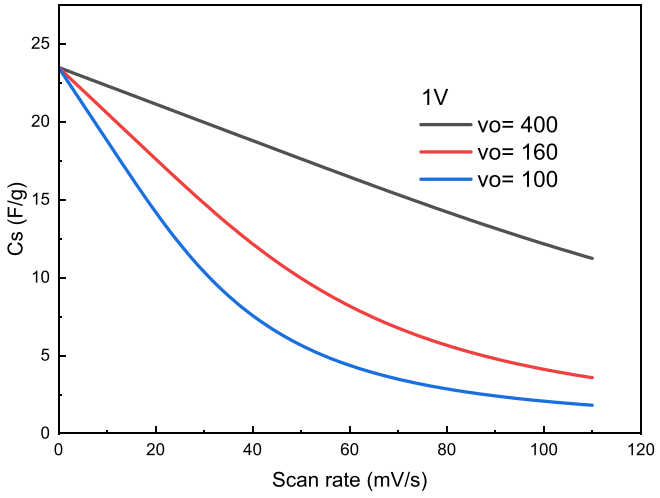

Fig. 5. Dependence of capacitance on scanning rate for different values of v_o.

capacitance saturation occurs at higher applied potentials (refer to Fig. 6).

4. Experimental

Supercapacitors with various electrodes and electrolytes were prepared to test and validate the proposed model. The samples were subjected to cyclic voltammetry tests at different scan rates. Choline chloride (ChCl, 2-hydroxy-*N*, *N*, *N*-trimethyl-ethyl ammonium chloride, 99 %) and ethylene glycol ("EG" (1,2 ethanediol, 99.8 %) were used to prepare the eutectic ionic liquids. A mixture with a molar ratio of 1:2 for ChCl-EG was heated to approximately 80°C for >30 min until a homogeneous liquid was formed. Upon cooling the ionic liquid to 27 °C, it remained stable for long-term storage, reaching equilibrium with the air humidity. An aqueous solution of 1 M KOH was used for comparison. The preparation of the activated carbon (*AC*) electrodes, for making the supercapacitors, was performed as the following description: Approximately 100 mg (57%) of material underwent a grinding process ($< 53\ \mu m$), then mixed with 12.5 mg (7%) of Vulcan XC-72-R (Cabot Corporation) (or carbon black) and 64 mg (36%) of polytetrafluoroethylene (PTFE with 60%H_2O :$\sim$ 40 mg of PTFE). Isopropyl alcohol (isopropanol; C_3H_8O) was used as the diluent during homogenization of the mixture. Vulcan XC-72-R was first mixed with PTFE to form a conductive binder and then added to the mixture, which was referred to as CA. During the homogenization step, the mixture was maintained in isopropanol and subsequently evaporated in an oven ($\sim 80^{\circ}C$). The already dried mixture was pressed ($2T/cm^2$) in a hard metal matrix ($\phi = 14mm$) for 2 min. Electrodes with 80 $\sim$ 95 mg of active material were adhered to a $\phi = 14\ mm$ diameter current collector using silver conductive glue. The supercapacitors were assembled using a porous filter paper as a separator for the electrodes, which were held together with the fasteners of an insulating material and soaked in the electrolyte for 36 h. A commercial organic supercapacitor was used as the standard reference. Table 3 lists the supercapacitors and their nomenclature. Cyclic voltammetry (CV) was performed using an Arbin BT-4 computerized analyzer ARBIN BT-4 using MitsPro version 4 software. For the cyclic voltammetry assays, scanning rates ranging from 1 to 100 mV/s were used.

5. Results and discussion

Rigorous experimental validation is essential to ensure reliability and relevance for practical applications. In this part of the study, was validated the mathematical model of the R-C circuit by manufacturing double-layer electrical capacitors. As a preliminary test, the current curve was simulated as a function of time using eq. (12). Fig. 7 shows the current curve as a function of time (Fig. 7a) for a commercial supercapacitor to which a scan rate of 5 mV/s was applied in the cyclic voltammetry test. The corresponding voltammograms are shown in Fig. 7b. To obtain the capacitance curves as functions of the scan rate, the model was fitted to the experimental points. Following the procedure described in Section 3, eq. 21 was used.

Figs. 8–11 represent the results of the adjustments made to the proposed model. A satisfactory reproduction of the experimental data trend was observed in the manner in which the capacitance decreased with the scan rate. The fitting parameters are shown in Tables 3, 4, and 5. To obtain an optimal fit, *ESR* (or v_o) must be considered as a variable that depends on the scan rate. The trend of this dependence of the ESR on the scan rate is shown in Figs. 8b, 9b, 10b, and 11b, which indicate that the ESR values decrease with an increase in the scan rate. This suggests that the *ESR* is related to the depth of charge penetration through the pores of the capacitor electrodes. The higher the scan rate, the lower the penetration depth for a given time. Thus, it is expected that the ions must travel a longer ohmic path at low scan rates than at higher scan rates. The same occurs for the porous surface of ions when an electric double layer is formed. This is in agreement with the lower capacitance and *ESR* values observed at high scan rates. However, the higher *ESR* values observed at low scan rates did not increase

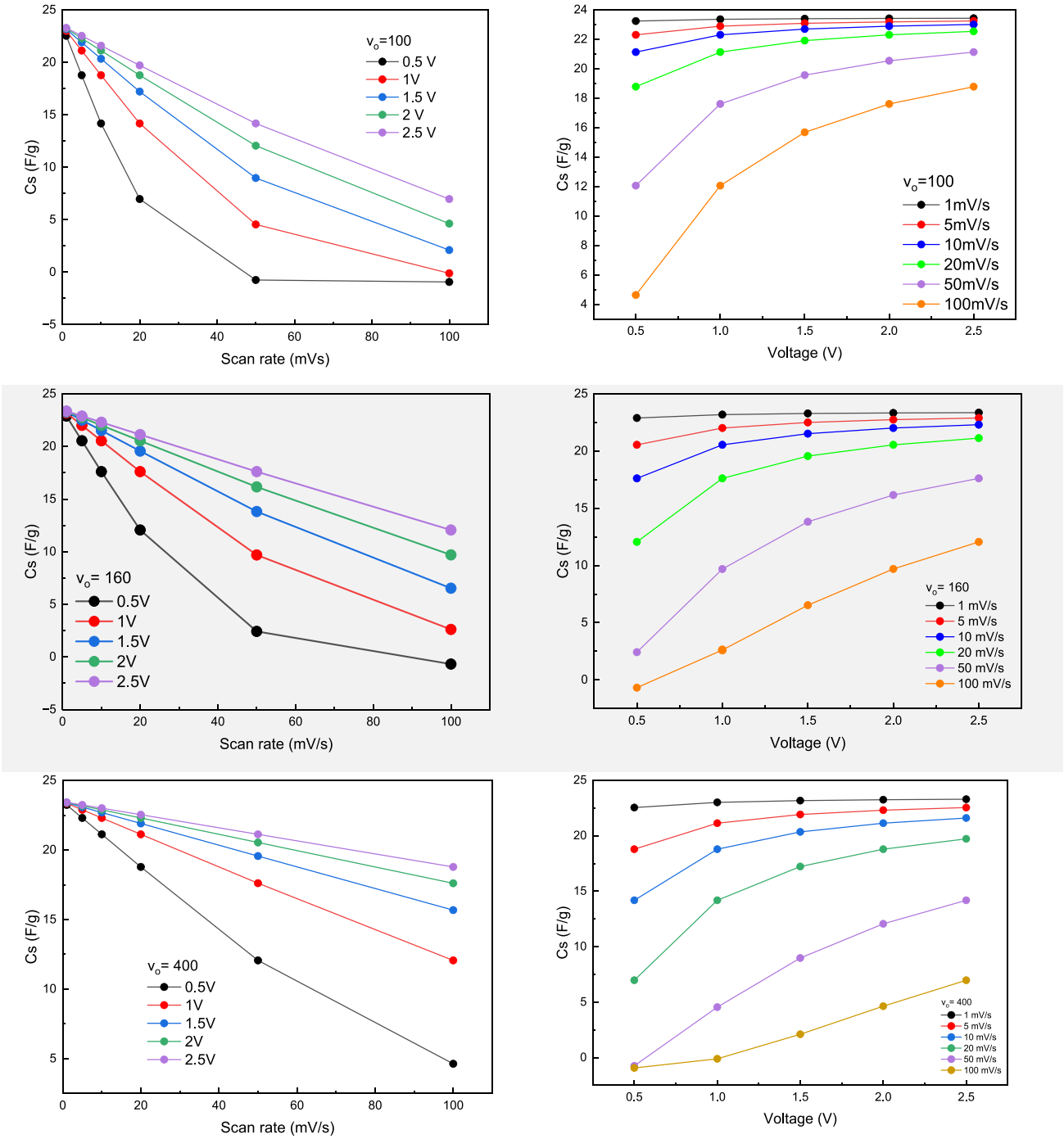

Fig. 6. Dependence of capacitance on scanning rate and dependence of capacitance on maximum applied voltage for the values of v_o used in Fig. 3

Table 3
Nomenclature of the tested supercapacitors.

Name	Electrode	Electrolyte
AC1	AC	CHClEG
AC2	AC	KOH
rGO1	rGO	KOH
Commercial	AC	Organic

indefinitely as the scan rate decreased. The latter is related to the finite electrode thickness, which results in the *ESR* not increasing indefinitely as the scan rate approaches zero.

Table 4 shows all parameters that resulted from fitting the model to the experimental data for the curves shown in Figs. 8, 9, 10, and 11. For an accurate analysis of the calculated *parameters,* the percentage variation of ESR_1 and ESR_2 (refer to Table 5) was calculated, as well as found a comparative ratio between the values of C_o and the capacitance obtained at the scan rate of 30 mV/s (refer to Table 6).

As a comparison between the present and previous adjustments [9], we highlight that the respective voltammogram adjustments were equivalent in terms of accuracy. In addition, the previous study considered EPR, whereas this study did not. This corroborates the present hypothesis that EPR has a negligible influence on the determination of the capacitance by cyclic voltammetry.

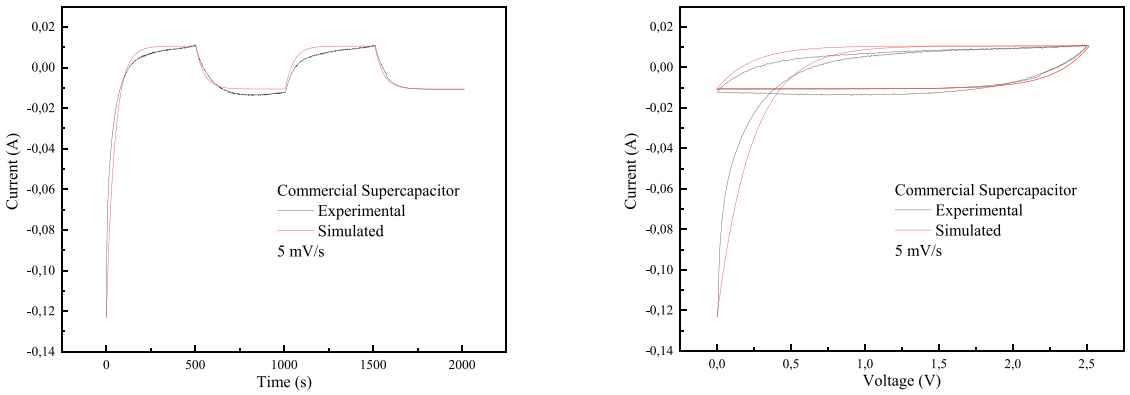

Fig. 7. a) current vs. time curve and b) voltammogram of a commercial supercapacitor fitted with eq. 12.

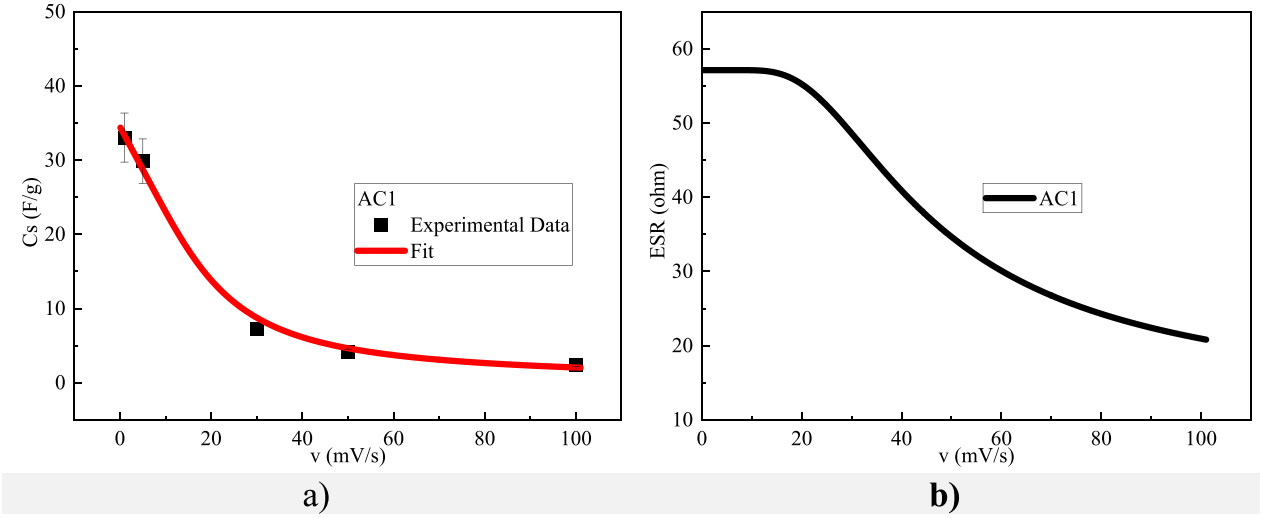

Fig. 8. Capacitance a) and ESR b) curves. Comparison of experimental data with the model

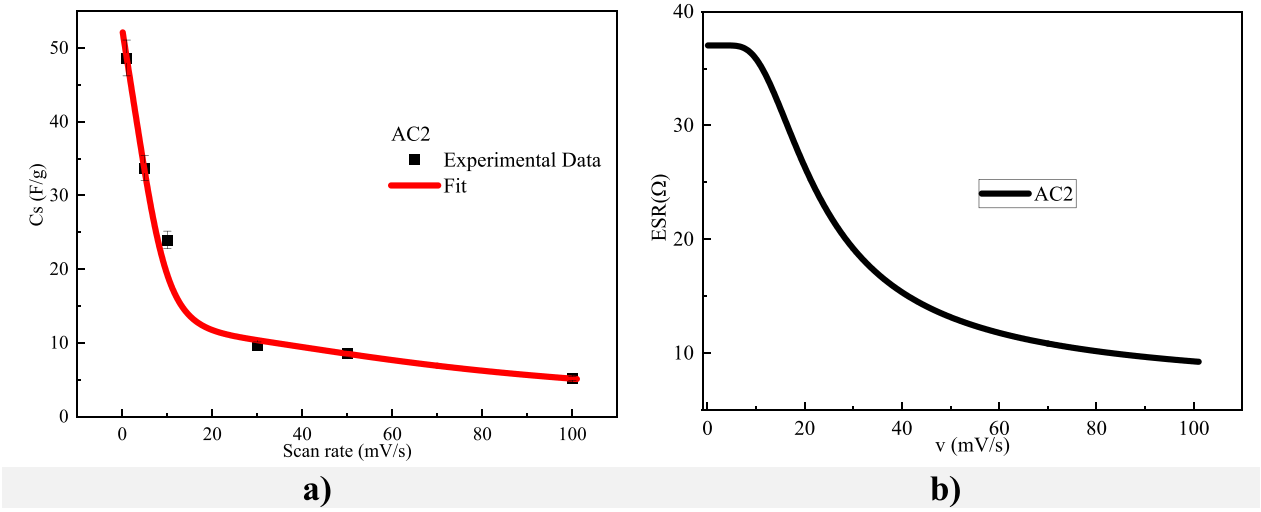

Fig. 9. Capacitance a) and ESR b) curves. Comparison of experimental data with the model.

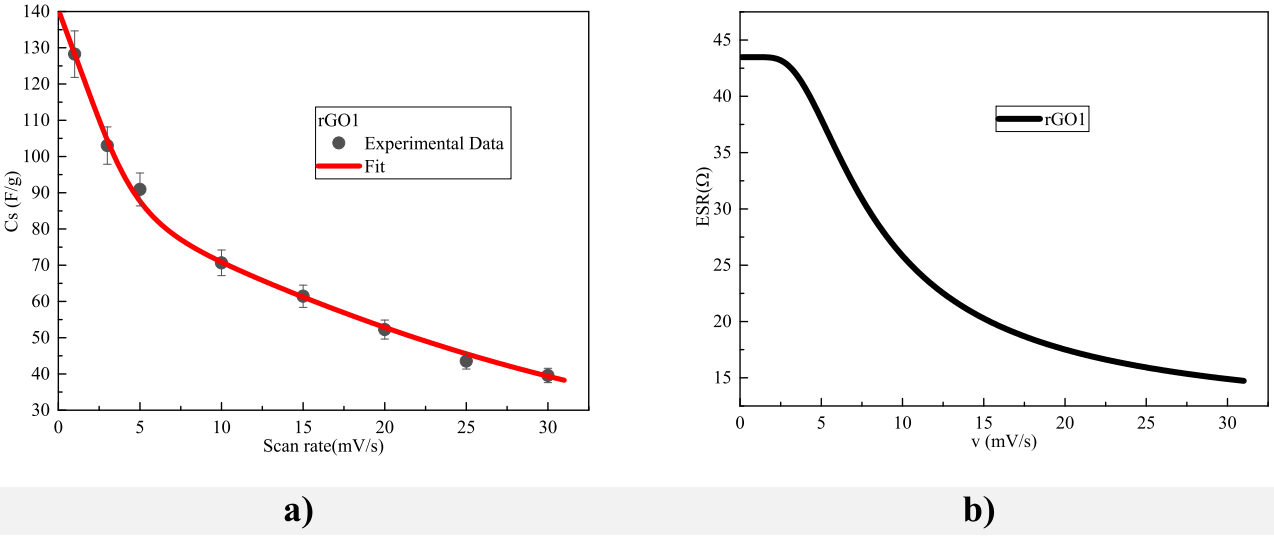

Fig. 10. Capacitance a) and ESR b) curves. Comparison of experimental data with the model.

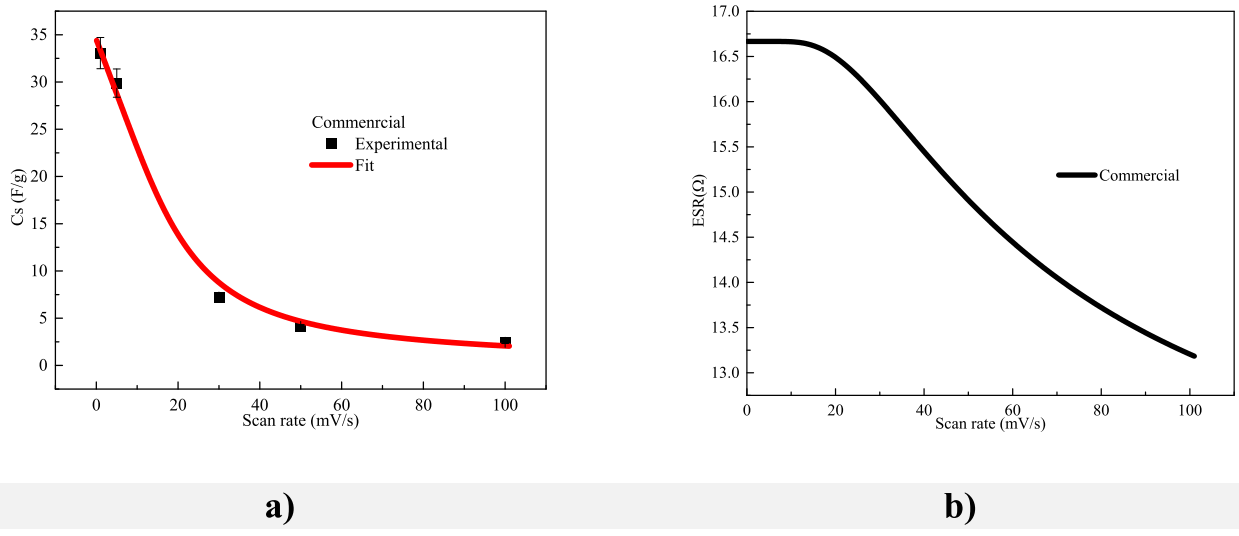

Fig. 11. Capacitance a) and ESR b) curves. Comparison of experimental data with the model.

Table 4
Fit parameters obtained from the model of all samples studied.

Sample	C_o(F/g)	v_{01}	$ESR_1(\Omega)$	v_{02}	$ESR_2(\Omega)$	v_{trans}
AC1	51	17.5	57.1	98	10.2	60
AC2	52.5	27	37.0	160	6.3	50
rGO1	140.5	23	43.5	97	10.3	15.5
Commercial	34.5	60	16.7	95	10.5	80

Table 5
Percentage variation of ESR parameters corresponding to low and high scan rates.

Sample	$ESR_1(\Omega)$	$ESR_2(\Omega)$	$\left(\frac{\Delta ESR}{ESR}\right)\%$
AC1	57.1	10.2	139
AC2	37.0	6.3	142
rGO1	43.5	10.3	123
Commercial	16.7	10.5	46

Table 6
Comparative ratio of the decrease in capacitance to the increase in v

Sample	C_o(F/g)	C (at 30 mV/s)	Co/C(at 30 mV/s)
AC1	51	4.9	10.4
AC2	52.5	8.5	6.2
rGO1	140.5	40	3.5
Commercial	34.5	7.1	4.9

For the present model to work properly it had to be assumed that the ESR decreases as the scan rate increases. At this juncture it is not possible to prove that this physically happens inside of the porous electrodes.

The specific capacitance versus scan rate was predicted using an artificial neural network [11]. It was shown that doping heteroatoms onto the carbon surface does not always increase the capacitance. The complicated relationship between capacitance and structural features, as well as the surface composition related to chemical doping, was discussed using experimental data from the literature. The experimental data for the pristine carbon electrode with a micropore surface area of 636 m^2/g and mesopore surface area 442 m^2/g were compared with

another of zero m^2/g pristine carbon micropore electrode and mesopore surface area of 24 m^2/g. The former showed a better curve than the latter. The doped carbon electrode (O = 7.87 at.%, N5 = 0.9447 at.%, N6 = 1.1139 at.%, NQ = 0.6651 at.%) with a micropore area of 1227 m^2/g and mesopore area of 1170 m^2/g showed excelent capacitance versus scan rate characteristics. No other reports on the microstructural pore features of the electrodes are available in the literature.

The potential application of the proposed approach has impact on the design and optimization of supercapacitors for specific industrial and scientific applications. Thus, by systematically varying only the scan rate of various supercapacitors it is possible to verify which electrical parameters are necessary to be altered as well, which would lead to better prediction of practical capacitors behavior.

6. Conclusions

The proposed model explains the commonly observed experimental behavior of the dependence of the supercapacitor capacitance on the scan rate. The model comprised a serial RC_o circuit in which the zero-scan-rate capacitance was considered a constant value, and the ESR turned into a fitting parameter that depended on the scan rate. It was observed that the ESR decreased between 60 % and 140 % with an increasing scan rate. The lowest variation was observed in the commercial supercapacitors, which could be due to the uniformity in the pore size and better adequacy in the choice of the corresponding electrolyte in relation to the manufactured supercapacitors. However, for scan rates approaching zero, the ESR values did not increase indefinitely but tended to plateau at a constant value. Regarding the decrease in capacitance with increasing scan rate, the rate of decrease depended on the combination of electrode material and electrolyte. In addition, the aqueous electrolyte KOH 1 M combines better with the graphene oxide electrode than with the activated carbon electrode. This could be due to the finite size of the electrode compared with the size of the electrolyte ions, which limited the maximum ESR and capacitance values. It was assumed that the dependence of the capacitance and serial resistance on the scan rate is probably related to the ion diffusion rate within the electrode pores. Although this model allows for a reasonable fit of a given voltammetry curve and the dependence of the capacitance on the scan rate by adjusting only the ESR, it is not possible to establish the possible intrinsic dependence of the capacitance on voltage.

CRediT authorship contribution statement

Fernando Gabriel, Jara Benitez: Writing – review & editing, Writing – original draft, Methodology, Investigation, Formal analysis, Data curation. **Alejandro Jorge, Bardella Peruzzi:** Writing – original draft, Methodology, Formal analysis, Data curation, Conceptualization. **Rubens Nunes Faria:** Supervision, Project administration.

Declaration of competing interest

The authors declare that they have no known competing financial interests or personal relationships that could have appeared to influence the work reported in this paper.

Data availability

Data will be made available on request.

Acknowledgements

The financing of the whole PhD program was supported by the National Scholarship Programme ``Don Carlos Antonio Lopez - BECAL`` of the Ministry of Economy and Finance of the Government of the Republic of Paraguay. Contract number: 171/2019.

References

[1] B.K. Kim, S. Sy, A. Yu, J. Zhang, Electrochemical supercapacitors for energy storage and conversion, in: Handbook of Clean Energy Systems, John Wiley & Sons, Ltd, Chichester, UK, 2015, pp. 1–25, https://doi.org/10.1002/9781118991978.hces112.

[2] G. Xiong, C. Meng, R.G. Reifenberger, P.P. Irazoqui, T.S. Fisher, A review of graphene-based electrochemical microsupercapacitors, Electroanalysis 26 (2014) 30–51.

[3] A.G. Pandolfo, A.F. Hollenkamp, Carbon properties and their role in supercapacitors, J. Power Sources (2006), https://doi.org/10.1016/j.jpowsour.2006.02.065. Preprint at.

[4] S. Zhang, N. Pan, Supercapacitors performance evaluation, Adv. Energy Mater. 5 (2014) 1401401.

[5] W. Raza, et al., Recent advancements in supercapacitor technology, Nano Energy 52 (2018) 441–473.

[6] K.R. Wehmeyer, R.M. Wightman, Scan rate dependence of the apparent capacitance at microvoltammetric electrodes, J. Electroanal. Chem. Interfacial Electrochem. 196 (1985) 417–421.

[7] S. Ardizzone, G. Fregonara, S. Trasatti, "Inner" and "outer" active surface of RuO2 electrodes, Electrochim. Acta 35 (1990) 263–267.

[8] Y. Ge, X. Xie, J. Roscher, R. Holze, Q. Qu, How to measure and report the capacity of electrochemical double layers, supercapacitors, and their electrode materials, J. Solid State Electrochem. 24 (2020) 3215–3230.

[9] A.P.R. Fernandez, E.A. Périgo, R.N. Faria, Analytical expressions for electrochemical supercapacitor with potential dependent capacitance, J Energy Storage 43 (2021) 103156.

[10] I.N. Jiya, N. Gurusinghe, R. Gouws, Electrical circuit modelling of double layer capacitors for power electronics and energy storage applications: A review, Electronics (Switzerland) 7 (2018), https://doi.org/10.3390/electronics7110268. Preprint at.

[11] M. Zhou, A. Vassallo, J. Wu, Data-driven approach to understanding the in-operando performance of heteroatom-doped carbon electrodes, ACS Appl Energy Mater 3 (2020) 5993–6000.